CHAPTER 5

TiO_2-zeolite composite modified Fe^0 nanoparticles for the removal of Cr(VI) and malachite green dye from water

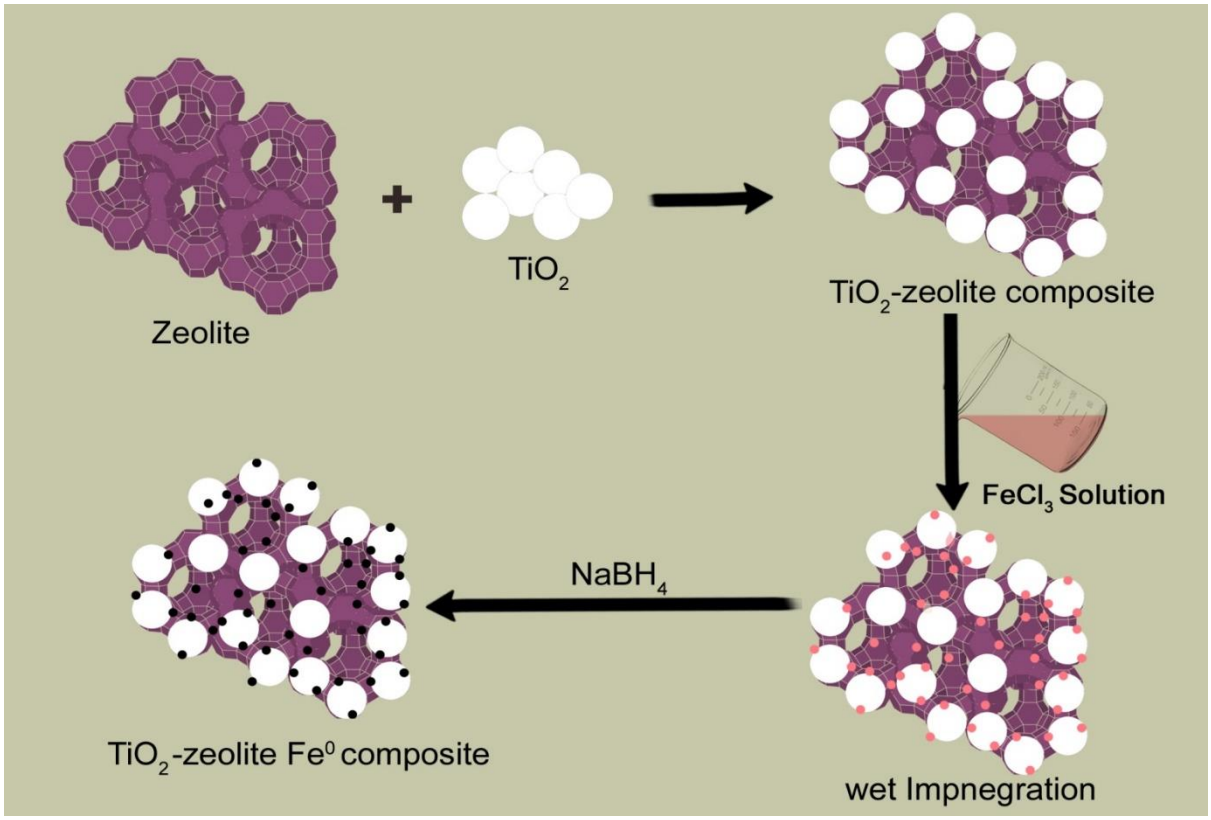

Chapter 5

TiO_2-zeolite composite modified Fe^0 nanoparticles for the removal of Cr(VI) and malachite green dye from water

5.1. Introduction

The search for the most suitable material for the remediation of water pollutants is a never-ending process. As discussed in previous chapters, zero valent iron (Fe^0) nanoparticle is an appropriate material for water remediation. However, the stability of Fe^0 nanoparticles is still a complicated issue. The rapid oxidation of the Fe^0 nanoparticles by reacting with air, moisture and non-targeted pollutants make them hard to handle. As per literature, TiO_2 can be used to retard the corrosion of metals and metal alloys[1]. In addition to this, TiO_2 is used for the adsorption of heavy metals[2], dyes[3] etc. and it is also used as a photocatalyst in various studies due to its chemical and photochemical stability, quantum confinement effect, strong resistance to acids and alkalis, large surface area to volume ratio along with low cost and low toxicity[4,5]. Efraim et al. used TiO_2 as a photocatalyst to degrade the antibiotic oxacillin through hydroxyl radicals created in the valence band of the former through photogenerated holes. In their study, around 90 % of the total organic carbon was removed by TiO_2 based photocatalysis[6]. Former studies show that Fe^{3+} doping of TiO_2 reduces the TiO_2 band gap since the Ti^{4+} ions in the crystal lattice are substituted by Fe^{3+} ions. The doping can shift the absorption of TiO_2 from the UV region to the visible region.

The charge carrier recombination rate gets reduced and the hydroxyl radical production has improved in Fe^{3+} doped TiO_2 photocatalyst. This leads to the enhanced photocatalytic degradation of the organic pollutant under UV and visible light illumination[7]. The presence of metal ions/metal nanoparticles in the TiO_2 surface improves photocatalytic activity and can act as electron scavengers to catch the photogenerated electrons[8]. This property will be helpful for the stabilization of Fe^0 nanoparticles for more extended periods. Even though the TiO_2 nanoparticles can be used for water treatment, they show high colloidal stability in water and are difficult to separate and recover after use[9].

The disadvantages of TiO_2 nanoparticles can be overcome by immobilizing them on a suitable support, which helps easy removal and separation after use. One of the

inexpensive and non-toxic supports for metal/metal oxide nanoparticles are zeolites (Z). Zeolites are three-dimensional aluminosilicate frameworks that show high surface area, abundant surface active sites for adsorption and excellent ion exchange capacity. More than that, it is resistant to the attack of hydroxyl radicals and effective even after recycling many times. It is important to note that the negative surface charges of the zeolites help them to show a high affinity towards cationic species[10]. The modification of zeolite by TiO_2 has been studied over the years. Different methods were used to establish TiO_2 nanoparticles on the surface of the zeolite. The most common method is growing TiO_2 nanoparticles on the zeolite matrix. Qing et al. produced TiO_2 nanoparticles supported on natural zeolite by the hydrolysis of $TiCl_4$[11]. Yan-Huei et al. prepared TiO_2-zeolite composite by wetness impregnation method in which the components are mixed, sonicated and finely sprayed on the hot glass plate[12]. In another study, Daryoush et al. synthesized NaX zeolite stabilized MgO–TiO_2 nanocomposite using the ultrasound-assisted dispersion method. The MgO and TiO_2 nanoparticles were mixed with NaX zeolite in water followed by sonication, stirring, drying, and calcination, giving NaX/MgO–TiO_2 nanocomposite [13].

In the present study, TiO_2-zeolite composite was prepared by the hydrothermal method and these composites were used to stabilize Fe^0 nanoparticles. The major objectives of the study are (1) preparation of TiO_2-zeolite composite (T-Z) with varying TiO_2 dosage, (2) synthesis of Fe^0 nanoparticles supported on TiO_2 nanoparticles, natural zeolite and TiO_2-zeolite composites, (3) characterization of the prepared composites and nanoparticles and (4) malachite green dye and Cr(VI) removal studies by prepared nanoparticles.

5.2. Experimental details

5.2.1 Preparation TiO_2-zeolite stabilized Fe nanoparticles

Preparation of TiO_2-zeolite Composites

The TiO_2-zeolite composite was prepared by depositing TiO_2 nanoparticles on the zeolite surface. At first, clean the purchased natural zeolite to remove organic impurities present in it. This is attained through sonication of zeolite in water followed by calcination at 600^{o}C for 6 hours in a muffle furnace. The subsequent cooling at room temperature and powdering using pestle and mortar provide refined zeolite particles. The TiO_2-zeolite composite was prepared by mixing specific weight percentages of purchased TiO_2 nanoparticles with clean zeolite powder in a 10 % ethanolic aqueous medium. This

solution was sonicated using a probe sonicator for 30 minutes and kept at 120^{o}C for 6 hours in a teflon-lined stainless steel autoclave. After that, the autoclave was cooled down at room temperature and washed with demineralised water. The TiO_2-zeolite composite was further calcinated at 600^{o}C for 6 hours and powdered using pestle and mortar. The 25 % TiO_2 nanoparticles loaded zeolite (25-T-Z) and 50 % TiO_2 nanoparticles loaded zeolite (50-T-Z) were prepared by maintaining the TiO_2 and zeolite particles ratio at 25:75 and 50:50 respectively.

Synthesis of stabilized Fe nanoparticles

The TiO_2-zeolite-Fe composite was prepared by the wet impregnation followed by liquid phase reduction method. For this, $FeCl_3.6H_2O$ (1 g) was dissolved in 10 mL of water and added 0.5 g of T-Z into it. The solution was stirred for 30 minutes and evaporated the solvent using a hot plate. The obtained material was powdered, weighed and redispersed in 10 mL of water and stirred 30 minutes under the nitrogen atmosphere. $NaBH_4$ solution was prepared by dissolving 0.5 g in 50 L of water and added dropwise to the solution. The appearance of a black precipitate indicates the formation of Fe^0 nanoparticles in the TiO_2-zeolite matrix. The precipitate was collected by vacuum filtration, washed with acetone, lyophilized and stored in airtight vials. In the synthesis of 25-T-Z-Fe, the 25-T-Z composite was used and for 50-T-Z-Fe preparation, the composite 50-T-Z was used. A similar procedure was followed to prepare T-Fe and Z-Fe nanoparticles in which TiO_2 nanoparticles and zeolite were used as stabilizing agents.

5.2.2 Batch experiments

Cr(VI) removal studies

The details of batch experiments followed for Cr(VI) removal were discussed in chapter 2. Different parameters examined in this study for Cr(VI) removal were nanoparticle dosage (0.4-1 g/L), initial concentration of Cr(VI) (1-7 mg/L), initial pH of the solution (4-10) and contact time (10-40 min). The pH of the solution has been adjusted using 1.0 M NaOH and 1.0 M H_2SO_4. All the experiments were performed with a duplicate.

Dye removal studies

The method followed for the MG dye removal batch experiment was already mentioned in chapter 3. The parameter studied in the present study were nanoparticle dosage (0.16-0.4 g/L), initial concentration of dye (10-50 mg/L), initial pH of the solution (5-9) and

contact time (15-60 min). The volume of dye solution taken was 25 mL and all the experiments were performed with a duplicate. The residual dye concentration was evaluated by UV-visible spectroscopy.

5.2.3 Characterisation and analytical techniques used

The prepared nanoparticles were lyophilised using Operon FDU 7003 lyophiliser. The characteristics of TiO_2 nanoparticles, zeolite and TiO_2–zeolite composites and corresponding iron nanoparticles were examined by HRTEM, UV-visible spectroscopy, EDAX, XRD and FTIR. Details of characterisation techniques were discussed in chapter 2. UV-visible spectrometer UV-2600, Shimadzu, Japan, was used to study the absorbance of TiO_2 nanoparticles, zeolite and TiO_2–zeolite composites and corresponding iron nanoparticles. Fourier transform infrared spectra of the prepared composite and corresponding Fe nanoparticles were investigated through Spectrum Two Fourier transform infrared spectrometer (FTIR, Perkin Elmer, USA). Jeol 6390LA/OXFORD XMX N was used for the elemental analysis of T-Fe, Z-Fe, 50-T-Z and 50-T-Z-Fe nanoparticles. GC-MS/MS analysed the degradation products of MG dye using 25-T-Z-Fe nanoparticles. The procedure followed for the GC-MS/MS analysis was discussed in chapter 3.

5.3. Results and discussion

5.3.1 Characterisation of the prepared materials

XRD

X-ray diffractogram of TiO_2 nanoparticles, zeolite powder, 25 % TiO_2 loaded zeolite composite and 50 % TiO_2 loaded zeolite composite was shown in figure 5.1. The powder XRD pattern of TiO_2 exhibited strong diffraction peaks at $2\theta = 25.7^o$ (101), 38.3^o (004), 48.49^o (200), 54.49^o (105) and 55.44^o (211) corresponding to the anatase phase of TiO_2[14]. The diffraction peaks observed at $2\theta = 69.31^o$ (031) and 70.5 (112) indicated the presence of the rutile phase of TiO_2 in lower percentages (JCPDS no 98-018-6186). Anatase TiO_2 nanoparticles show superior photocatalytic property compared to rutile TiO_2. In the XRD spectrum of zeolite, the peaks shown at 30.3^o, 27.4^o, 24.3^o, 22.0^o and 10.5^o corresponds to the clinoptilolite zeolite[15,16]. The XRD peaks of 25-T-Z and 50-T-Z have a similar pattern of TiO_2 and zeolite, with a slight shift in the XRD peaks. With the increase in TiO_2 dosage, the peaks of zeolite were decreased drastically. This indicates that zeolites are covered with TiO_2 nanoparticles completely. Figure 5.2 shows the XRD

pattern of Fe nanoparticles stabilised on the TiO_2 nanoparticles, zeolite, 25-T-Z and 50-T-Z composites. XRD peak at 45.4º indicates (110) plane of the zero valent iron, which is present in all the four Fe nanoparticles[17]. The intense peak at 31.7º corresponds to the (104) plane of α-Fe_2O_3[18]. The other peaks in the T-Fe, Z-Fe, 25-T-Z-Fe and 50-T-Z-Fe nanoparticles were that of the corresponding stabilising agent, TiO_2 and zeolite, with a slight shift in their peak position.

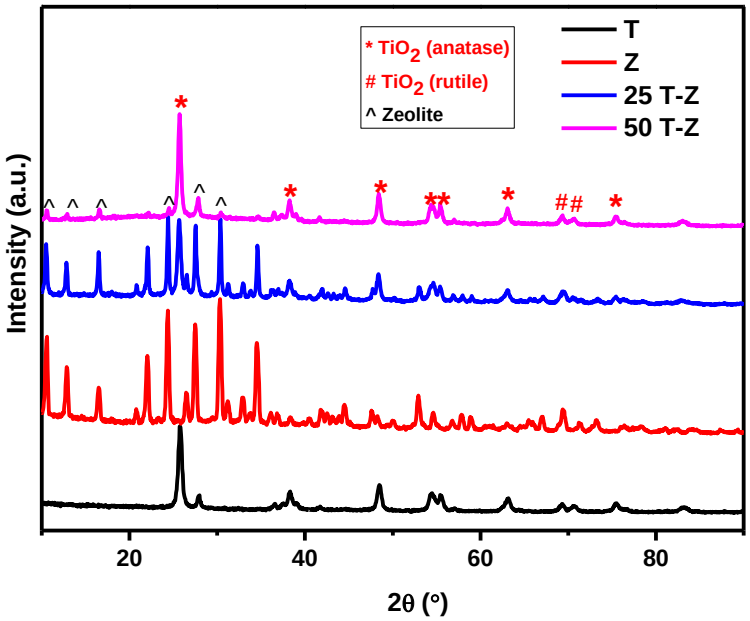

Figure 5.1 *XRD pattern of TiO_2 nanoparticles, zeolite, 25-T-Z and 50-T-Z composite*

The high peak intensity of Fe^0 in 50-T-Z-Fe and T-Fe nanoparticles indicates the efficient stabilization of Fe^0 in these matrices. This is mainly due to the involvement of TiO_2 nanoparticles. Typically, TiO_2 nanoparticles are photocatalytically active in the UV region. However, its activity can be shifted to the visible region through the doping of Fe[19]. Electrons get excited to the conduction band of TiO_2 from its valence band when exposed to UV radiation. This leads to the formation of electron-hole pairs within the system. The lifetime of these excited electron-hole pair determines the photochemistry of TiO_2. Photocatalytic activity of TiO_2 is minimized as the excited electrons in the conduction band recombines with the holes in the valence band. This charge recombination could be minimized by coupling TiO_2 with materials that can accept the electrons from the conduction band. According to Eleni et al., the iron oxide shell of the Fe^0 nanoparticles can act as electron trappers that accept the photoexcited electron from

the conduction band of TiO_2, thereby reducing Fe^{3+} to Fe^{2+}. The interaction between TiO_2 and Fe retard the thicker iron oxide layer formation and gives longer reactivity of Fe^0 nanoparticles in TiO_2 matrices[8]. The incorporation of zeolite enhanced the efficiency of TiO_2 nanoparticles, which may be due to the more dispersibility of TiO_2 nanoparticles in the zeolite matrix. Previous studies show that the photocatalytic activity of TiO_2 can be enhanced using zeolite as a supporting agent. Guangxin et al. synthesized TiO_2-zeolite composite and applied it to degrade gaseous and aqueous organic pollutants. They detected high efficiency for the degradation of organic pollutants which is attributed to high surface area of TiO_2-zeolite composite[20]. In the case of 50-T-Z-Fe, the TiO_2 nanoparticles were more dispersed in zeolite matrix and may show high surface area. This leads to the improved stabilization Fe^0 in 50-T-Z-Fe nanoparticles.

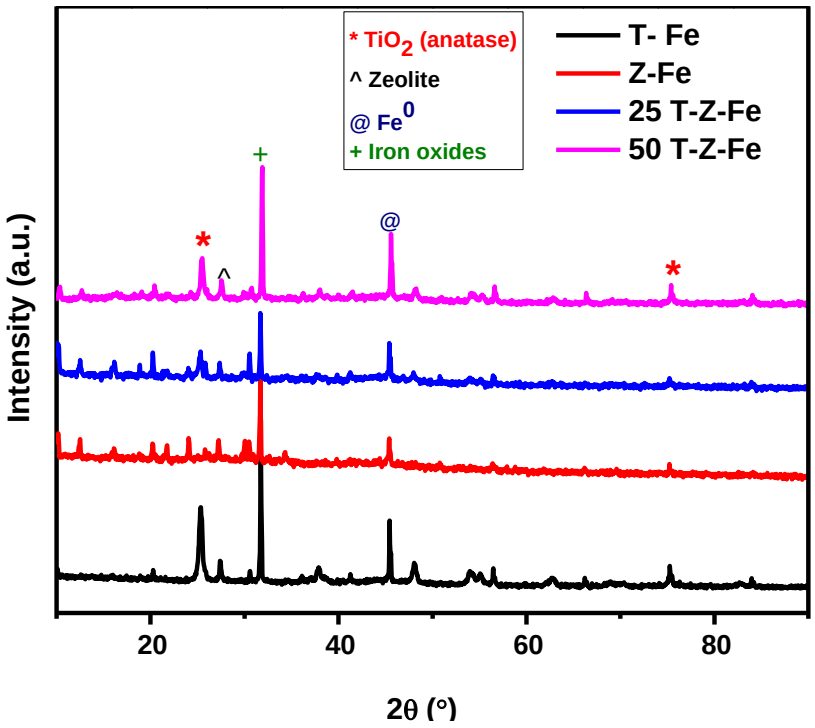

Figure 5.2 *XRD pattern of T-Fe, Z-Fe, 25-T-Z-Fe and 50-T-Z-Fe nanoparticles*

HRTEM

Figure 5.3 represents the HRTEM image and SAED pattern of 50-T-Z and 50-T-Z-Fe respectively. As shown in figure 5.3a, the TiO_2 nanoparticles were deposited on the surface of the zeolite. The particle size of TiO_2 ranges between 20-35 nm with an average particle size of 25 nm and the size of zeolite particles is around 150 nm. The 50-T-Z materials show the crystalline property, which is evident from the SAED pattern. Figure 5.3b envisages that the Fe^0 nanoparticles with particle size below 20 nm were deposited on the

surface of TiO_2 nanoparticles. The Fe nanoparticles exhibit a shell of iron oxide which may arise due to the oxidation of nanoparticles. The SAED pattern of 50-T-Z-Fe shows that the nanoparticles display crystalline properties similar to the 50-T-Z.

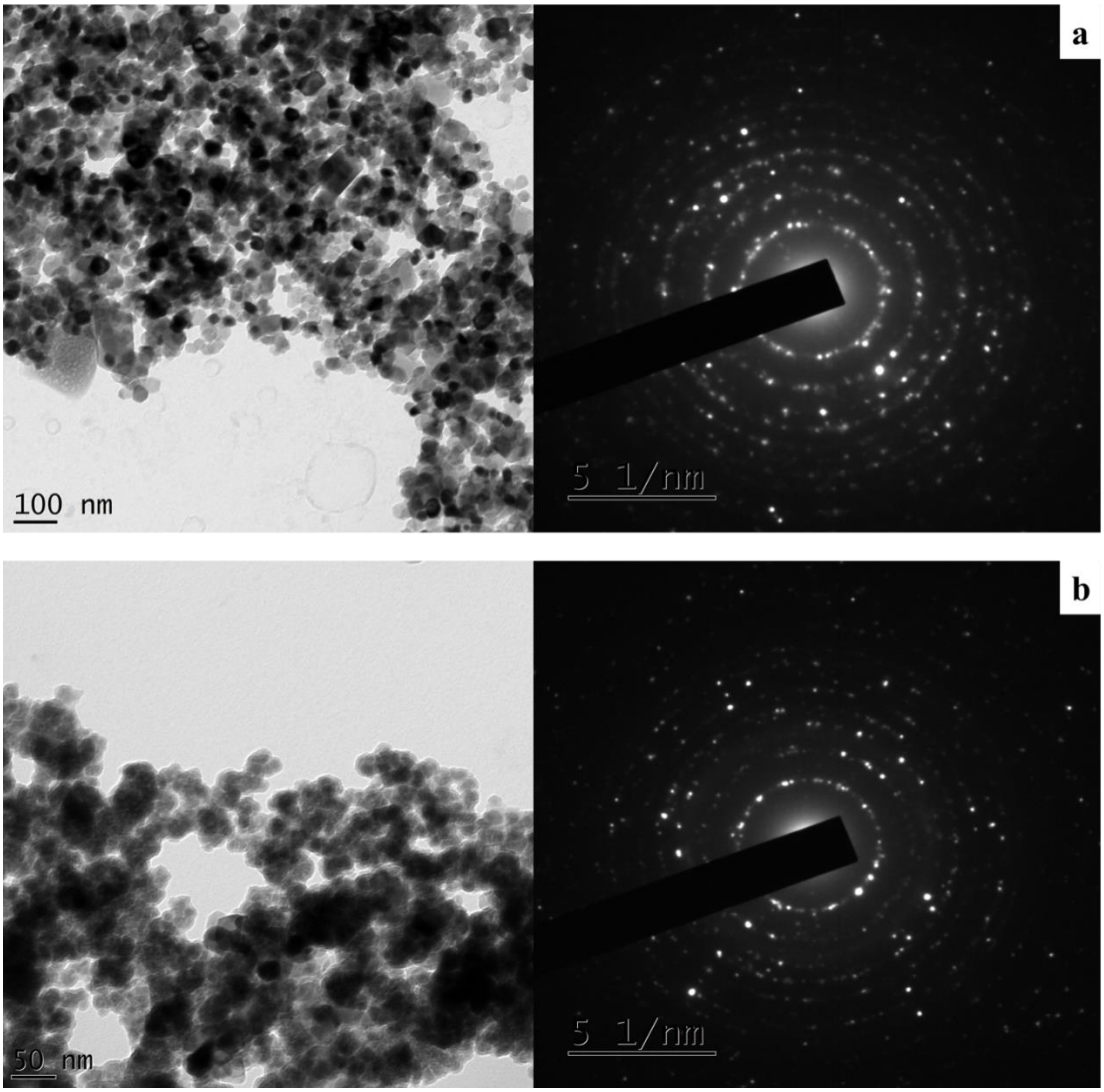

Figure 5.3 *HRTEM image SAED pattern of 50-T-Z (a) and 50-T-Z-Fe nanoparticles*

EDAX

EDAX spectra and mapping of T-Fe, Z-Fe, 50-T-Z and 50-T-Z-Fe nanoparticles were shown in figure 5.4 (a, b, c & d) and figure 5.5 (a, b, c & d) respectively. EDAX spectra confirm the presence of respective elements in prepared nanoparticles; for example, T-Fe contains Ti, O and Fe, Z-Fe contains Al, Si, O and Fe, 50-T-Z contains Al, Si, O and Ti, and 50-T-Z-Fe contains Al, Si, O, Ti and Fe elements. As shown in figure 5.4, the percentage of oxygen is less in 50-T-Z-Fe compared to T-Fe and Z-Fe, which shows that 50-T-Z protects Fe^0 more efficiently than TiO_2 and zeolite. In accordance with the EDAX

spectra, the atomic weight percentage of Fe in T-Fe, Z-Fe and 50-T-Z-Fe nanoparticles were 15 %, 16 % and 20 % respectively. The EDAX mapping of prepared nanoparticles gives information about the distribution of Fe nanoparticles in TiO_2, zeolite, 25-T-Z and 50-T-Z matrices. The iron nanoparticles were uniformly distributed in TiO_2 and 50-T-Z surfaces. In the case of Z-Fe, the Fe nanoparticles were more present in zeolite channel/cavities than surfaces as indicated by the reduced intensity of Fe in Z-Fe nanoparticles (figure 5.5b).

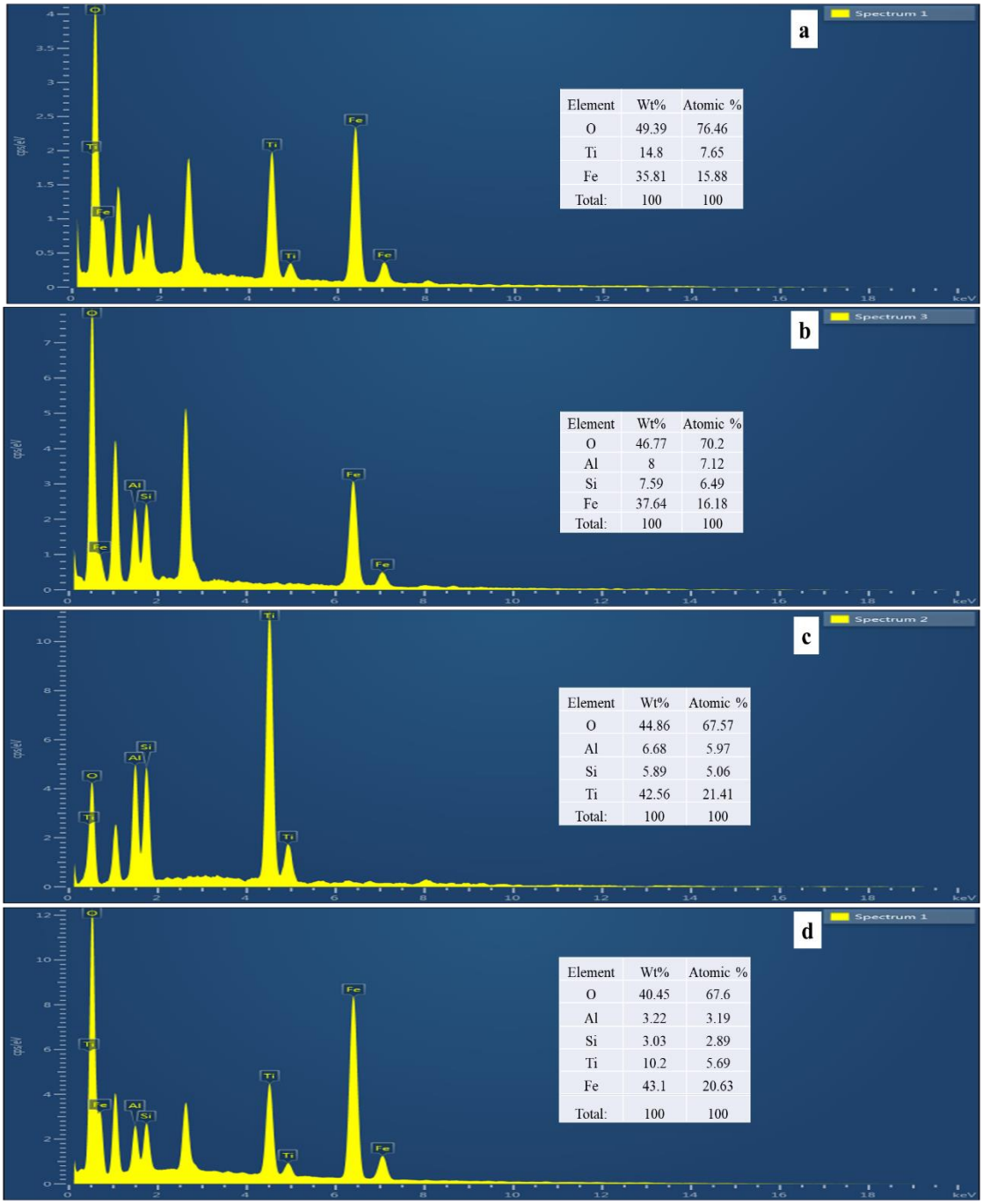

Figure 5.4 *EDAX spectra of (a) T-Fe, (b) Z-Fe, (c) 50-T-Z and (d) 50-T-Z-Fe*

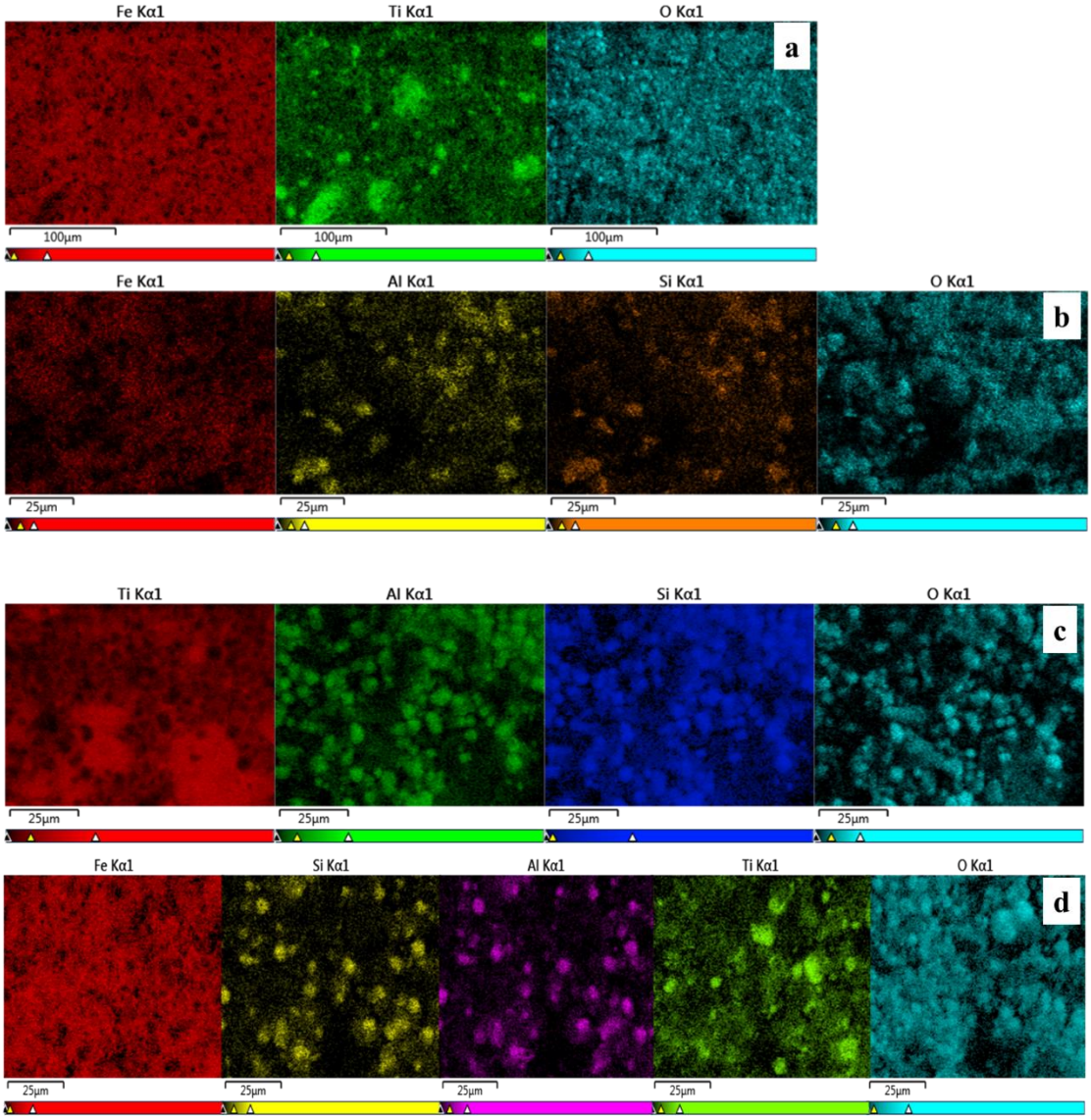

Figure 5.5 *EDAX mapping of (a) T-Fe, (b) Z-Fe, (c) 50-T-Z and (d) 50-T-Z-Fe*

FTIR

Figure 5.6 represents the FTIR spectra of T-Fe, Z-Fe, 25-T-Z-Fe and 50-T-Z-Fe nanoparticles and their corresponding stabilizing materials. The interaction between Fe^0 and stabilizing materials were established using FTIR measurements. Figure 5.6a represents the FTIR spectra of TiO_2 and T-Fe nanoparticles. The peak centred at 3479 cm^{-1}, belonging to the stretching vibration of the -OH group due to the absorption of moisture from the atmosphere. The peak at 730 cm^{-1} corresponding to the O–Ti–O bonding of TiO_2 anatase nanoparticles shifted to 694 cm^{-1} in T-Fe nanoparticles[21]. This confirms the incorporation of Fe in TiO_2 lattice since the red shift is a sign of structural defect in TiO_2 lattice. In figure 5.6b, the existence of zeolite can be confirmed by the peaks between

400-850 cm^{-1}[22]. The shift in peak position from 1365 cm^{-1} to 1350 cm^{-1} suggests the interaction of Fe nanoparticles with zeolite. The peak centred around 980 cm^{-1} is due to the vibration of Si-O or Al-O of the zeolite is split into two peaks due to the replacement of Si with Fe during the Fe deposition. The zeolite peaks at 663 cm^{-1} were blue-shifted to 696 cm^{-1} in Z-Fe nanoparticles. This also supports the interaction of zeolite with Fe^0 nanoparticles. A similar trend has also been seen in 25-T-Z-Fe and 50-T-Z-Fe nanoparticles too. The FTIR spectra of 25-T-Z and 50-T-Z exhibit the peaks of TiO_2 and zeolite. The introduction of Fe shifted the peaks to higher/lower wavenumber.

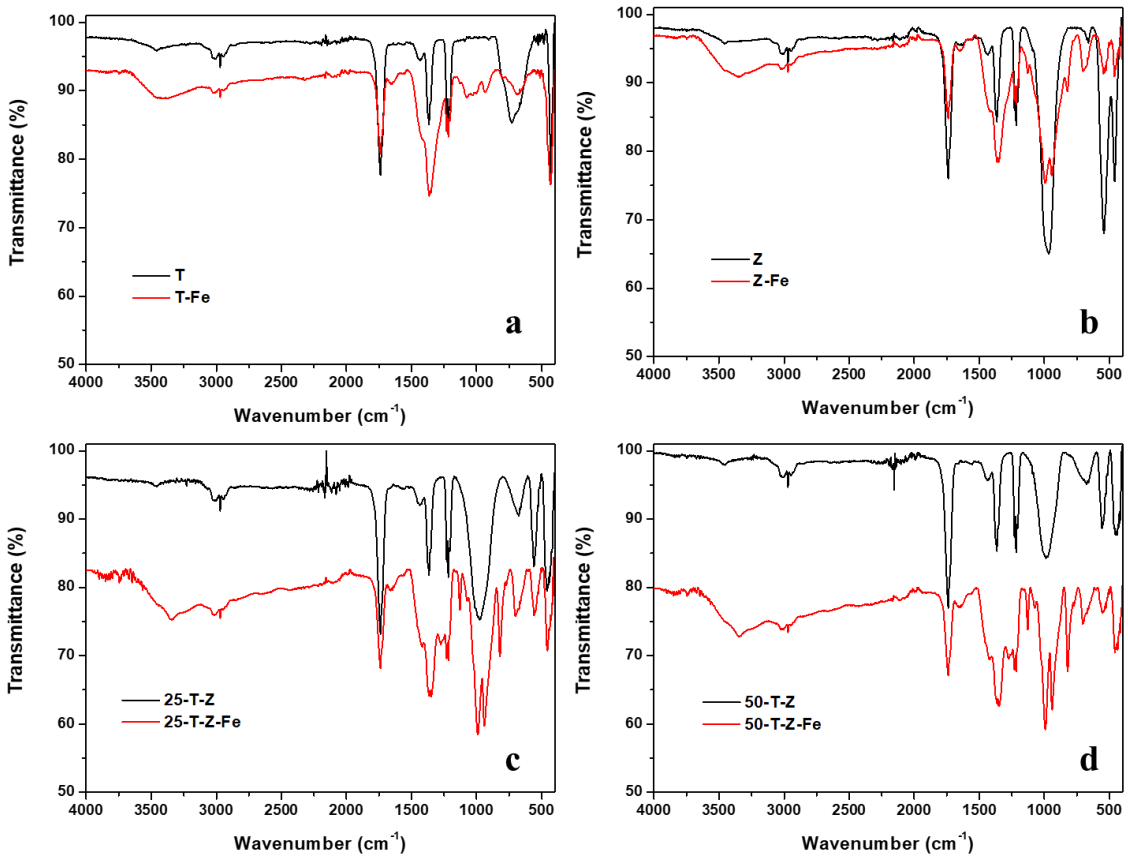

Figure 5.6 *FTIR spectra of (a) TiO_2 and T-Fe nanoparticles, (b) zeolite and Z-Fe nanoparticles, (c) 25-T-Z and 25-T-Z-Fe nanoparticles and (d) 50-T-Z and 50-T-Z-Fe nanoparticles*

UV-visible spectroscopy

TiO_2 exhibited its characteristic absorption maxima in the UV region as observed by UV-visible spectroscopy (figure 5.7). The absorbance spectrum of zeolite also reveals its characteristic absorbance in the UV region of spectra. A considerable shift in peak intensity and position occurred in the absorption spectra of TiO_2 and zeolite with the

incorporation of Fe. The presence of Fe in TiO_2, decreased the intensity of absorption of the latter in the UV region and enhanced the absorption of TiO_2 in the visible region. This red shift in the peak position of TiO_2 in T-Fe is depicted in figure 5.7a. On the other hand, the spectra of Z-Fe composite displayed enhanced absorption intensity in UV and the visible region compared to that of pristine zeolite. All these observations support the existence of molecular interaction between TiO_2 as well as zeolite with Fe. The presence of Fe extended the absorption of TiO_2 and zeolite to the visible region. Similar reconstructions were observed in the absorption bands of T-Z composites (25 T-Z-Fe and 50 T-Z-Fe) with the association of Fe. The extension of absorption of TiO_2, Zeolite and T-Z to visible region in the presence of Fe also suggests the possibility of these composites to exhibit their photocatalytic activity in the visible region too.

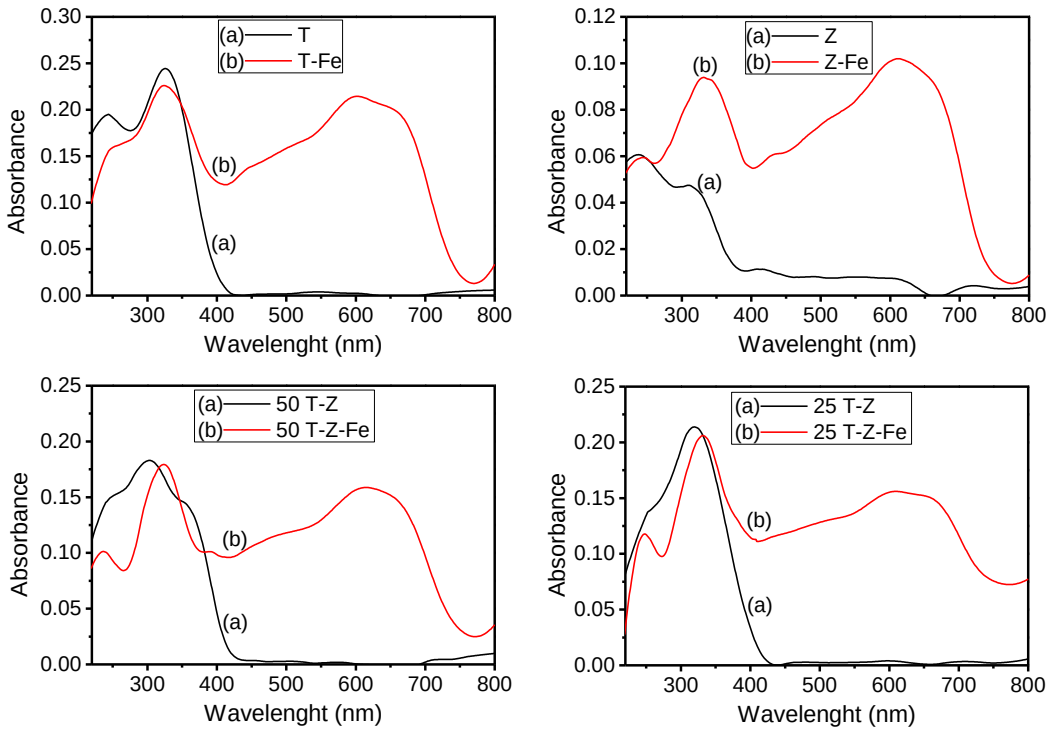

Figure 5.7 *UV-visible spectra of T-Fe, Z-Fe, 25-T-Z-Fe and 50-T-Z-Fe nanoparticles in comparison with TiO_2 and zeolite*

5.3.2 Cr(VI) removal studies

Cr(VI) removal studies have been done using T-Fe, Z-Fe, 25-T-Z-Fe and 50-T-Z-Fe nanoparticles and are shown in figure 5.7. The results show that 25-T-Z-Fe and 50-T-Z-Fe nanoparticles exhibit the highest removal efficiency compared to T-Fe and Z-Fe nanoparticles. This indicates the presence of more Fe^0 in 25-T-Z-Fe and 50-T-Z-Fe than

T-Fe and Z-Fe nanoparticles. The improved efficiency of Z-Fe over T-Fe may be due to the adsorption of Cr(VI) ions onto the empty cavities/channels of zeolite. The synergetic activity of zeolite and TiO_2 significantly reduced the oxidation probability of Fe^0 nanoparticles and enhanced the adsorption properties of 25-T-Z-Fe and 50-T-Z-Fe nanoparticles. The existence of TiO_2 nanoparticles also added some effect on Cr(VI) removal. TiO_2 nanoparticles exhibit photocatalytic activity in the visible region along with the UV region due to the doping of Fe[19]. So the absorption of visible light followed by the generation of electrons and holes also influenced the reduction of Cr(VI). The photogenerated electrons reduce the Cr(VI) to Cr(III) through redox reactions to some extent[23]. Some of the photogenerated electrons were trapped by the iron oxide shell and regenerated after the Cr(VI) reduction[8]. The synergetic photocatalytic effect of TiO_2 and zeolite adsorption significantly improved the Cr(VI) removal in 25-T-Z-Fe and 50-T-Z-Fe systems.

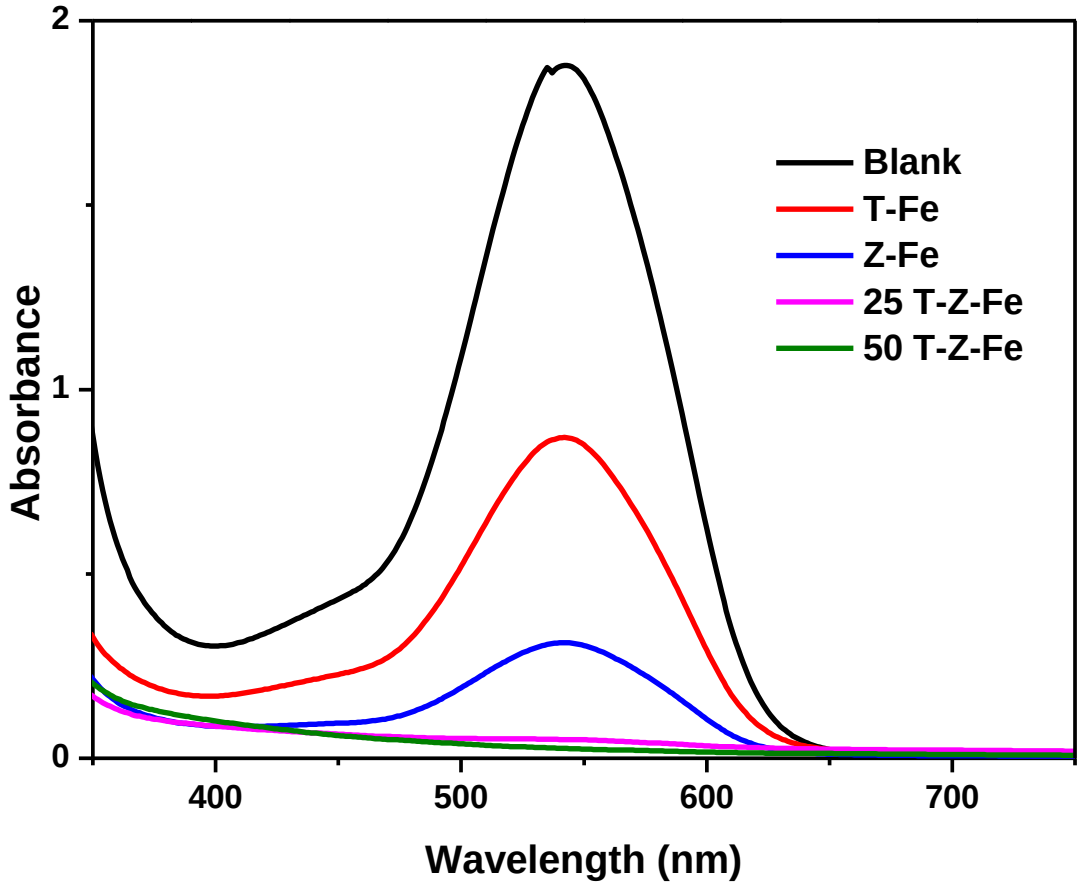

Figure 5.7 *UV-visible spectra of Cr(VI) after treating with T-Fe, Z-Fe, 25-T-Z-Fe and 50-T-Z-Fe nanoparticles*

Effect of nanoparticle dosage

Figure 5.8a represents the effect of nanoparticles dosage on the Cr(VI) removal using T-Fe, Z-Fe, 25-T-Z-Fe and 50-T-Z-Fe nanoparticles. The nanoparticles dosage varied between 0.4 g/L to 1 g/L maintaining the initial Cr(VI) concentration at 5 mg/L and with a 15 minute contact time. The results show the highest removal efficiency in 25-T-Z-Fe nanoparticles along with 50-T-Z-Fe nanoparticles and the lowest Cr(VI) removal efficiency exhibited by T-Fe nanoparticles. While using 0.8 g/L of nanoparticles, the T-Fe, Z-Fe, 25-T-Z-Fe and 50-T-Z-Fe nanoparticles show 78 %, 89 %, 95 % and 93 % of Cr(VI) removal efficiency respectively. The removal efficiency increased with the increase in nanoparticles dosage which is attributed to the high surface area and high surface active sites of prepared nanoparticles along with the rise in nanoparticles dosage. After the dosage of 0.8 g/L, the removal efficiency does not improve significantly. This may be due to the aggregation of nanoparticles.

Effect of the initial concentration of the Cr(VI) solution

The effect of the initial concentration of nanoparticles on the removal of Cr(VI) from water is shown in figure 5.8b. The nanoparticles dosage and contact time during the study were kept constant at 0.6 g/L and 15 minutes respectively. The results show that the removal efficiency decreased drastically with an increase in Cr(VI) concentration. The highest removal efficiency was exhibited in 1 mg/L Cr(VI) solution and the lowest by 7 mg/L Cr(VI) solution. In 1 mg/L solution, the T-Fe, Z-Fe, 25-T-Z-Fe and 50-T-Z-Fe nanoparticles show 81%, 93 %, 95 % and 95 % removal efficiency which is reduced to 49 %, 63 %, 78 % and 76 % at 7 mg/L solutions. This is due to the increase in the ratio between pollutant molecules and nanoparticle dosage, which leads to the decrease in the availability of surface active sites for the reduction of Cr(VI) ions.

Effect of contact time

As shown in figure 5.8c, the effect of contact time on Cr(VI) removal has been studied by keeping nanoparticles dosage (0.6 g/L) and initial Cr(VI) concentration (5 mg/L) constant. The results show that the 25-T-Z-Fe and 50-T-Z-Fe nanoparticles attained the maximum removal efficiency within 20 minutes of reaction time. However, in the case of T-Fe and Z-Fe nanoparticles, 30 minutes is needed to attain the maximum removal efficiency. This indicates that 25-T-Z-Fe and 50-T-Z-Fe nanoparticles reacted more actively with Cr(VI) ions than T-Fe and Z-Fe nanoparticles. At 40 minutes of contact time the T-Fe, Z-Fe, 25-

T-Z-Fe and 50-T-Z-Fe nanoparticles display 77 %, 87 %, 93 % and 92 % Cr(VI) removal efficiency.

Effect of pH

The effect of pH on Cr(VI) removal was studied and depicted in figure 5.8c. The results demonstrate that the pH has little effect on Cr(VI) removal for Z-Fe, 25-T-Z-Fe and 50-T-Z-Fe nanoparticles. However, the removal efficiency reduced significantly in T-Fe nanoparticles from acidic to basic pH. The high removal efficiency in low pH may be due to the high degree of protonation of prepared nanoparticles and the shredding of iron oxide shell in the prepared Fe^0 nanoparticles.

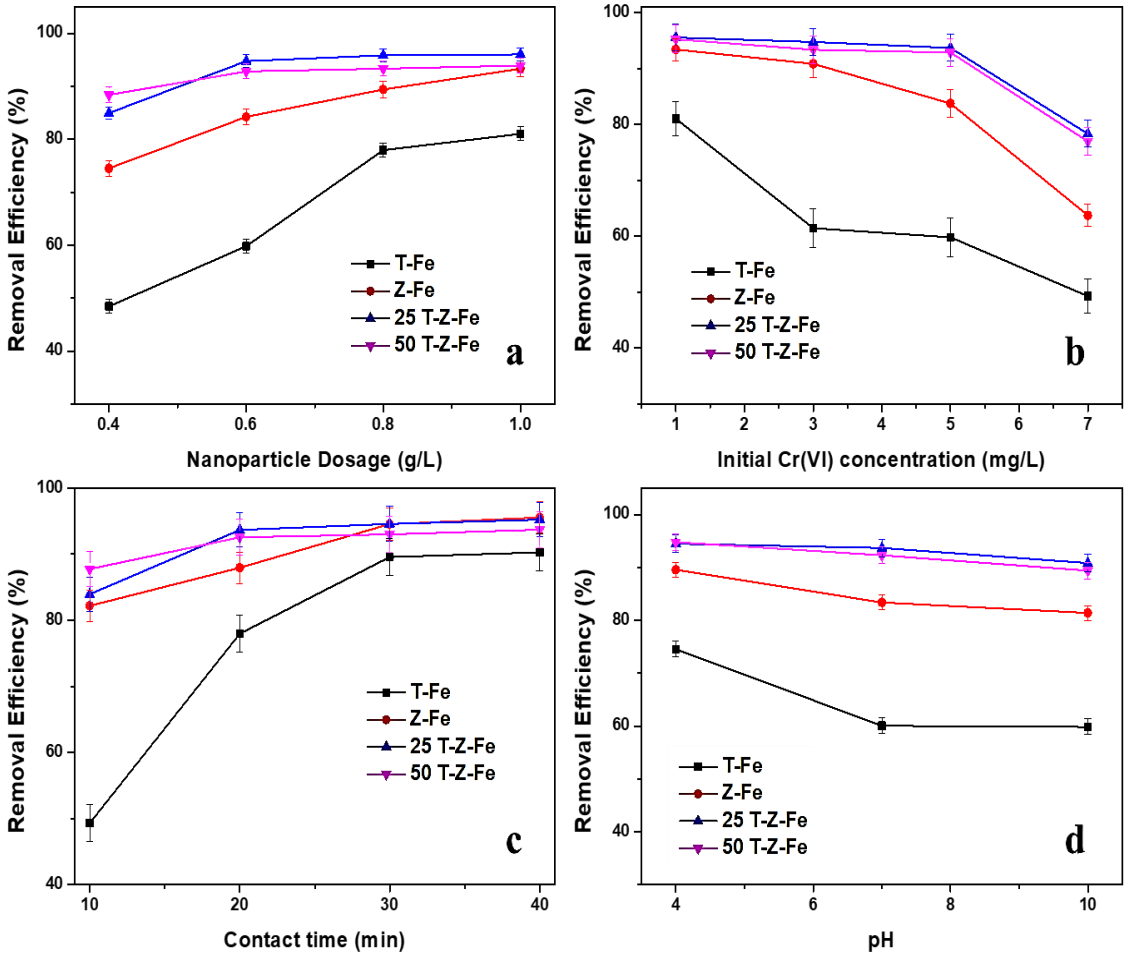

Figure 5.8 *(a) Effect of nanoparticle dosage, (b) Effect of initial concentration of Cr(VI), (c) Effect of contact time and (d) Effect of pH on Cr(VI) removal using T-Fe, Z-Fe, 25-T-Z-Fe and 50-T-Z-Fe nanoparticles*

5.3.3 MG dye removal studies

Malachite green dye removal studies have been done using T-Fe, Z-Fe, 25-T-Z-Fe and 50-T-Z-Fe nanoparticles and are depicted in figure 5.9. The highest removal efficiency was exhibited by 25-T-Z-Fe nanoparticles followed by 50-T-Z-Fe, T-Fe and Z-Fe nanoparticles. This is due to the enhanced electron transfer, production of reactive oxygen species and adsorption onto zeolite.

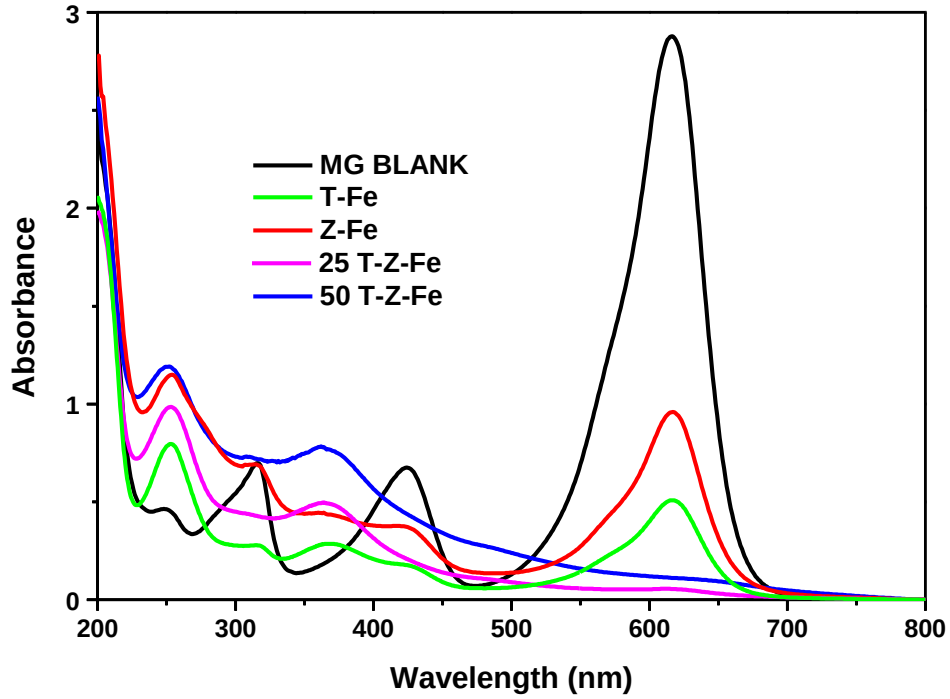

Figure 5.9 *UV-visible spectra of MG dye after treating with T-Fe, Z-Fe, 25-T-Z-Fe and 50-T-Z-Fe nanoparticles*

As discussed in chapter 3, Fe^0 nanoparticles degrade the malachite green dye molecules through reduction by direct electron transfer and atomic hydrogen and oxidation by reactive oxygen species such as hydroxyl radical. Along with the property of Fe^0, the stabilizing material is also involved in the removal of malachite green in T-Fe, Z-Fe, 25-T-Z-Fe and 50-T-Z-Fe nanoparticles. Previous studies show that malachite green was effectively adsorbed by zeolite through single layer adsorption and the intraparticle diffusion affected the adsorption rate of malachite green[24]. In addition to the adsorptive properties of zeolite, TiO_2 nanoparticles also played an important role in removing malachite green. Zulakha et al. effectively removed congo red dye using Fe_2O_3-titanium dioxide nanotubes under visible light[25]. This agrees with the previous assumption that Fe doped TiO_2 is an excellent photocatalyst compared to TiO_2 nanoparticles. The

photogenerated electrons can act as reducing agents and holes created by TiO_2 nanoparticles react with OH^- ions and form hydroxyl radicals. These hydroxyl radicals can act as excellent oxidizing agents for dye degradation[8]. Earlier, Meng et al. treated industrial dye wastewater using TiO_2–zeolite nanocomposites and they found that TiO_2–Zeolite nanocomposites were more effective than pristine TiO_2 particles. This is due to the adsorption-oriented photocatalytic degradation of dye molecules when using TiO_2–zeolite nanocomposites[26]. The synergetic effect of Fe^0 with TiO_2-zeolite in T-Z-Fe composite significantly enhances the dye removal.

Effect of nanoparticle dosage

The effect of nanoparticles dosage on dye removal has given in figure 5.10a. The quantity of nanoparticles added was varied from 0.16 g/L to 0.4 g/L with a constant initial concentration of dye (50 mg/L) and contact time (30 min). 90 % removal of dye molecules was attained by 25-T-Z-Fe nanoparticles followed by 50-T-Z-Fe (89 %), T-Fe (83 %) and Z-Fe (78 %) using 4 g/L of nanoparticles. With the increase in nanoparticles dosage, the MG removal efficiency increases due to the more direct electron transfer, formation of reactive oxygen species and increase in adsorption sites.

Effect of the initial concentration of the MG

The effect of the initial concentration of the MG dye was studied and shown in 5.10b. During the study, the nanoparticle dosage was taken as 0.32 g/L and contact time was kept as 30 minutes. The results show a decrease in MG removal efficiency with an increase in the initial concentration of dye molecules except in the case of 10 mg/L dye solution. This indicates that adsorption also played an important role in MG dye removal using prepared nanoparticles along with degradation. As expected, the dye removal efficiency decreased with the increased initial concentration of the dye, which may be due to the insufficient availability of surface active sites in a finite nanoparticle dosage.

Effect of contact time

The effect of contact time on the removal of MG dye molecules was studied (figure 5.10c.) by keeping nanoparticles dosage and initial concentration of the dye constant. The effect of contact time was studied in 15 minute time intervals and the results show that the 25-T-Z-Fe and 50-T-Z-Fe nanoparticles attained maximum removal efficiency within 15 minutes and the T-Fe and Z-Fe nanoparticles accomplished maximum removal efficiency

within 30 minutes. With the increase in contact time, the vacant adsorptive sites get occupied and the formation of reactive species gets reduced. This eventually reduced the removal efficiency of T-Fe, Z-Fe, 25-T-Z-Fe and 50-T-Z-Fe nanoparticles. The maximum removal efficiency attained by the prepared nanoparticles was 85 %, 74 %, 90 % and 89 % respectively, for T-Fe, Z-Fe, 25-T-Z-Fe and 50-T-Z-Fe nanoparticles.

Effect of pH

Figure 5.10d represents the effect of pH on the removal of MG dye using T-Fe, Z-Fe, 25-T-Z-Fe and 50-T-Z-Fe nanoparticles. The significant decrease in removal efficiency can be seen when the solution pH changes from acidic to basic. In acidic pH, the nanoparticles show 82 %, 81 %, 89 % and 89 % removal efficiency respectively for T-Fe, Z-Fe, 25-T-Z-Fe and 50-T-Z-Fe nanoparticles, which decreased to 63 %, 58 %, 79 % and 80 % in basic medium. This is due to the formation of the iron oxide layer, which reduces the reactivity of Fe^0 nanoparticles at higher pH.

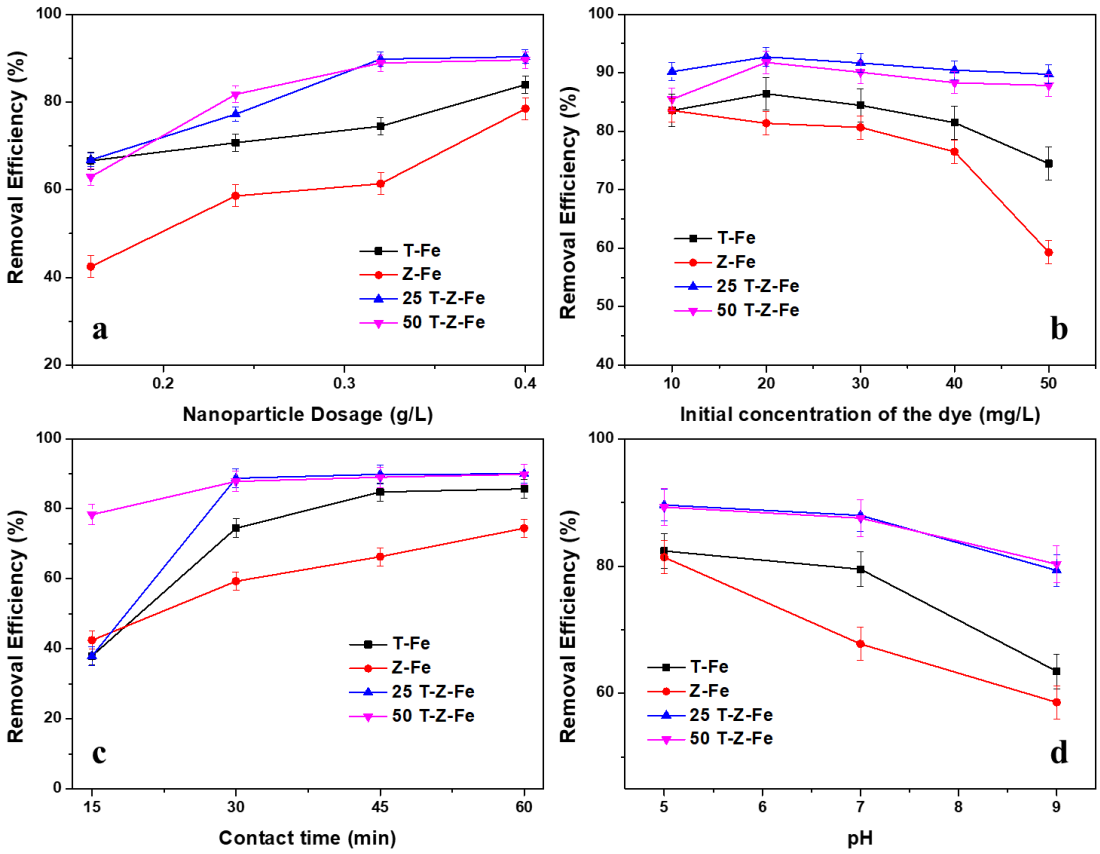

Figure 5.10 *(a) Effect of nanoparticle dosage, (b) Effect of initial concentration of MG, (c) Effect of contact time and (d) Effect of pH on MG dye removal using T-Fe, Z-Fe, 25-T-Z-Fe and 50-T-Z-Fe nanoparticles*

GC-MS/MS analysis

The GC-MS/MS analysis has been done on MG dye's degradation product, which is treated with the 25-T-Z-Fe nanoparticles. The GC-MS/MS analysis identified four degradation products of MG as (a) cyclohexa-2,5-diene-1,4-dione (MW 108), (b) diphenylmethanone (MW 182), (c) 3-(dimethylamino)phenol (MW 137) and (d) [4-(dimethylamino)phenyl]-phenylmethanone (MW 225) using the NIST library. The degradation products cyclohexa-2,5-diene-1,4-dione and diphenylmethanone were already reported in MG/Fe^0 system (chapter 3). However, the 3-(dimethylamino)phenol (R_t 15.81) and [4-(dimethylamino) phenyl]-phenylmethanone (R_t 21.27) were not reported by GC-MS/MS analysis in the previous chapters and figure 5.11 a & b represents the mass spectra of respective degradation products. The hydroxyl radical attack causes the degradation of MG into [4-(dimethylamino)phenyl]-phenylmethanone and N,N-dimethylaniline. The N,N-dimethyl aniline further transformed into 3-(dimethylamino)phenol through hydroxyl addition reaction[28]. Scheme 5.1 represents the formation of 3-(dimethylamino)phenol from N,N-dimethylaniline.

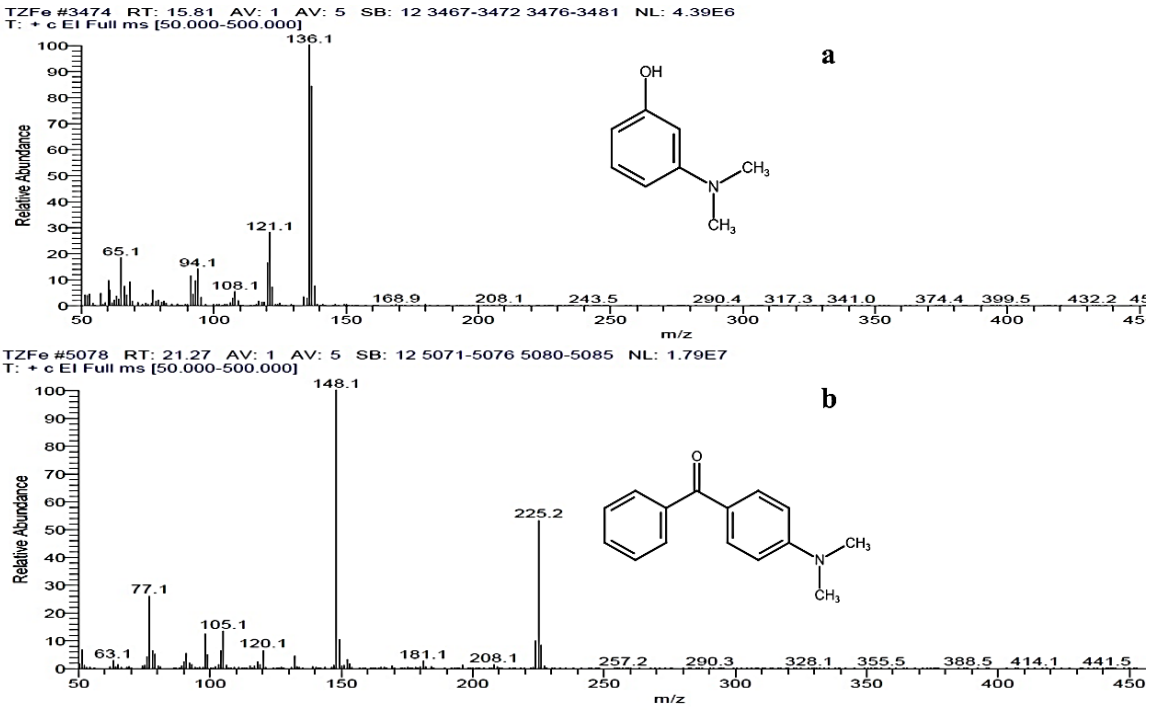

Figure 5.11 *Mass spectra of MG degradation products identified by GC-MS/MS analysis a) 3-(dimethylamino)phenol and b) [4-(dimethylamino)phenyl]-phenylmethanone*

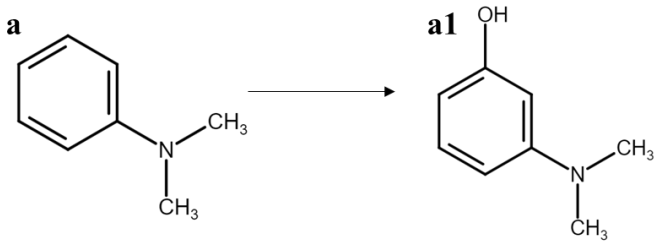

Scheme 5.1 *Degradation pathways of MG using 25-T-Z-Fe nanoparticles*

5.4. Conclusion

In this study, TiO_2-zeolite composite was used to stabilize Fe^0 nanoparticles. The TiO_2-zeolite composite was prepared by sonication followed by the hydrothermal method. The Fe^{3+} was incorporated in TiO_2-zeolite composite by wet impregnation and synthesized Fe^0 nanoparticles by liquid-phase reduction. The characterization of TiO_2-zeolite composite and T-Z-Fe nanoparticles have been done by XRD, FTIR, UV-visible spectroscopy, EDAX and HRTEM. In the prepared nanoparticles, 25-T-Z-Fe and 50-T-Z-Fe nanoparticles show more removal efficiency for Cr(VI) and MG dye compared to T-Fe and Z-Fe nanoparticles. The removal efficiency increases with increasing nanoparticle dosage and contact time and decreasing the initial concentration of the pollutant and pH of the solution. The study envisages that among the iron nanoparticles prepared in TiO_2/zeolite composites, 25-T-Z-Fe is the most efficient material for the removal of environmental pollutants.

5.5. References

[1] A. Shanaghi, A.R. Sabour, T. Shahrabi, M. Aliofkhazraee, Corrosion protection of mild steel by applying TiO_2 nanoparticle coating via sol-gel method, Prot. Met. Phys. Chem. Surfaces. 45 (2009) 305–311. https://doi.org/10.1134/S2070205109030071.

[2] W. Zhang, L. Zou, L. Wang, Photocatalytic TiO_2/adsorbent nanocomposites prepared via wet chemical impregnation for wastewater treatment: A review, Appl. Catal. A Gen. 371 (2009) 1–9. https://doi.org/10.1016/j.apcata.2009.09.038.

[3] M. Abbas, Experimental investigation of titanium dioxide as an adsorbent for removal of Congo red from aqueous solution, equilibrium and kinetics modeling, J. Water Reuse Desalin. 10 (2020) 251–266. https://doi.org/10.2166/wrd.2020.038.

[4] S.-Y. Lee, S.-J. Park, TiO_2 photocatalyst for water treatment applications, J. Ind. Eng. Chem. 19 (2013) 1761–1769. https://doi.org/10.1016/j.jiec.2013.07.012.

[5] S. Riaz, S.-J. Park, An overview of TiO_2-based photocatalytic membrane reactors for water and wastewater treatments, J. Ind. Eng. Chem. 84 (2020) 23–41. https://doi.org/10.1016/j.jiec.2019.12.021.

[6] E.A. Serna-Galvis, J. Silva-Agredo, A.L. Giraldo, O.A. Flórez, R.A. Torres-Palma,

Comparison of route, mechanism and extent of treatment for the degradation of a β-lactam antibiotic by TiO 2 photocatalysis, sonochemistry, electrochemistry and the photo-Fenton system, Chem. Eng. J. 284 (2016) 953–962. https://doi.org/10.1016/j.cej.2015.08.154.

[7] H. Khan, I.K. Swati, Fe^{3+} -doped Anatase TiO 2 with d–d Transition, Oxygen Vacancies and Ti^{3+} Centers: Synthesis, Characterization, UV–vis Photocatalytic and Mechanistic Studies, Ind. Eng. Chem. Res. 55 (2016) 6619–6633. https://doi.org/10.1021/acs.iecr.6b01104.

[8] E. Petala, M. Baikousi, M.A. Karakassides, G. Zoppellaro, J. Filip, J. Tuček, K.C. Vasilopoulos, J. Pechoušek, R. Zbořil, Synthesis, physical properties and application of the zero-valent iron/titanium dioxide heterocomposite having high activity for the sustainable photocatalytic removal of hexavalent chromium in water, Phys. Chem. Chem. Phys. 18 (2016) 10637–10646. https://doi.org/10.1039/c6cp01013j.

[9] S. Mustapha, M.M. Ndamitso, A.S. Abdulkareem, J.O. Tijani, D.T. Shuaib, A.O. Ajala, A.K. Mohammed, Application of TiO_2 and ZnO nanoparticles immobilized on clay in wastewater treatment: a review, Appl. Water Sci. 10 (2020) 49. https://doi.org/10.1007/s13201-019-1138-y.

[10] J. Huang, S. Yi, C. Zheng, I.M.C. Lo, Persulfate activation by natural zeolite supported nanoscale zero-valent iron for trichloroethylene degradation in groundwater, Sci. Total Environ. 684 (2019) 351–359. https://doi.org/10.1016/j.scitotenv.2019.05.331.

[11] Q. Sun, X. Hu, S. Zheng, Z. Sun, S. Liu, H. Li, Influence of calcination temperature on the structural, adsorption and photocatalytic properties of TiO_2 nanoparticles supported on natural zeolite, Powder Technol. 274 (2015) 88–97. https://doi.org/10.1016/j.powtec.2014.12.052.

[12] Y.H. Jan, L.Y. Lin, M. Karthik, H. Bai, Titanium dioxide/zeolite catalytic adsorbent for the removal of NO and acetone vapors, J. Air Waste Manag. Assoc. 59 (2009) 1186–1193. https://doi.org/10.3155/1047-3289.59.10.1186.

[13] D. Mirzaei, A. Zabardasti, Y. Mansourpanah, M. Sadeghi, S. Farhadi, Efficacy of Novel NaX/MgO–TiO_2 Zeolite Nanocomposite for the Adsorption of Methyl Orange (MO) Dye: Isotherm, Kinetic and Thermodynamic Studies, J. Inorg. Organomet. Polym. Mater. 30 (2020) 2067–2080. https://doi.org/10.1007/s10904-019-01369-9.

[14] K. Kusdianto, M. Hudandini, D. Jiang, M. Kubo, M. Shimada, Effect of Heating Rate on the Photocatalytic Activity of Ag–TiO_2 Nanocomposites by One-Step Process via Aerosol Routes, Catalysts. 12 (2021) 17. https://doi.org/10.3390/catal12010017.

[15] S.M. Baghbanian, Synthesis, characterization, and application of Cu 2 O and NiO nanoparticles supported on natural nanozeolite clinoptilolite as a heterogeneous catalyst for the synthesis of pyrano[3,2-b]pyrans and pyrano[3,2-c]pyridones, RSC Adv. 4 (2014) 59397–59404. https://doi.org/10.1039/C4RA10537K.

[16] A. Kalantarifard, J.G. Gon, G.S. Yang, Formaldehyde Adsorption into Clinoptilolite Zeolite Modified with the Addition of Rich Materials and Desorption Performance Using Microwave Heating, Terr. Atmos. Ocean. Sci. 27 (2016) 865–875. https://doi.org/10.3319/TAO.2016.05.28.01(TT).

[17] W. Gao, D. Zhong, Y. Xu, H. Luo, S. Zeng, Nano zero-valent iron supported by macroporous styrene ion exchange resin for enhanced Cr(VI) removal from aqueous solution, J. Dispers. Sci. Technol. (2020) 1–11. https://doi.org/10.1080/01932691.2020.1848583.

[18] Y. Sun, B. Yang, Y. Tian, G. Guo, W. Cai, M. He, Y. Liu, Facile synthesis of Ag–Fe_2O_3 core–shell composite nanoparticles by an in situ method, Micro Nano Lett. 6 (2011) 82–

85. https://doi.org/10.1049/mnl.2010.0149.

[19] S. Sood, A. Umar, S.K. Mehta, S.K. Kansal, Highly effective Fe-doped TiO 2 nanoparticles photocatalysts for visible-light driven photocatalytic degradation of toxic organic compounds, J. Colloid Interface Sci. 450 (2015) 213–223. https://doi.org/10.1016/j.jcis.2015.03.018.

[20] G. Zhang, A. Song, Y. Duan, S. Zheng, Enhanced photocatalytic activity of TiO_2/zeolite composite for abatement of pollutants, Microporous Mesoporous Mater. 255 (2018) 61–68. https://doi.org/10.1016/j.micromeso.2017.07.028.

[21] S. Bagheri, K. Shameli, S.B. Abd Hamid, Synthesis and Characterization of Anatase Titanium Dioxide Nanoparticles Using Egg White Solution via Sol-Gel Method, J. Chem. 2013 (2013) 1–5. https://doi.org/10.1155/2013/848205.

[22] Y. Rashtbari, J.H.P. Américo-Pinheiro, S. Bahrami, M. Fazlzadeh, H. Arfaeinia, Y. Poureshgh, Efficiency of Zeolite Coated with Zero-Valent Iron Nanoparticles for Removal of Humic Acid from Aqueous Solutions, Water. Air. Soil Pollut. 231 (2020). https://doi.org/10.1007/s11270-020-04872-9.

[23] Y. Song, X. Lu, Z. Liu, W. Liu, L. Gai, X. Gao, H. Ma, Efficient Removal of Cr(VI) by TiO_2 Based Micro-Nano Reactor via the Synergy of Adsorption and Photocatalysis, Nanomaterials. 12 (2022) 291. https://doi.org/10.3390/nano12020291.

[24] M. Tanyol, Rapid malachite green removal from aqueous solution by natural zeolite: process optimization by response surface methodology, Desalin. WATER Treat. 65 (2017) 294–303. https://doi.org/10.5004/dwt.2017.20185.

[25] Z. Zafar, R. Fatima, J.-O. Kim, Effect of HCl treatment on physico-chemical properties and photocatalytic performance of Fe–TiO_2 nanotubes for hexavalent chromium reduction and dye degradation under visible light, Chemosphere. 284 (2021) 131247. https://doi.org/10.1016/j.chemosphere.2021.131247.

[26] M.N. Chong, Z.Y. Tneu, P.E. Poh, B. Jin, R. Aryal, Synthesis, characterisation and application of TiO_2-zeolite nanocomposites for the advanced treatment of industrial dye wastewater, J. Taiwan Inst. Chem. Eng. 50 (2015) 288–296. https://doi.org/10.1016/j.jtice.2014.12.013.

[27] S. Banerjee, M.C. Chattopadhyaya, Adsorption characteristics for the removal of a toxic dye, tartrazine from aqueous solutions by a low cost agricultural by-product, Arab. J. Chem. 10 (2017) S1629–S1638. https://doi.org/10.1016/j.arabjc.2013.06.005.

[28] V. Chaturvedi, P. Verma, Biodegradation of malachite green by a novel copper-tolerant Ochrobactrum pseudogrignonense strain GGUPV1 isolated from copper mine waste water, Bioresour. Bioprocess. 2 (2015). https://doi.org/10.1186/s40643-015-0070-8.